Numerical studies of physiological pulsatile flow through constricted tube

Wei Liao, T.S. Lee and H.T. Low
Department of Mechanical Engineering, National University of Singapore, Singapore

Received January 2003
Revised September 2003
Accepted September 2003

Keywords *Laminar flow, Simulation, Numerical analysis*

Abstract *A detailed analysis on the characteristics of laminar flow over a bell-shaped stenosis for a physiological pulsatile flow is presented in this study. In order to have a good understanding of the physiological pulsatile flow, a comparison of the numerical solutions to three types of pulsatile flows, including a physiological flow, an equivalent pulsatile flow and a pure sinusoidal flow, are made in this work. The comparison shows that the flow behavior cannot be properly estimated if the equivalent or simple pulsatile inlet flow is used in the study of flow fields through stenosed arteries instead of actual physiological one. Then the physiological pulsatile flow is further studied by considering the effect of constriction ratio of stenosis, Womersley number and Reynolds number on the flow behavior through stenosed arteries. The analysis shows that the variation of these flow parameters puts significant impacts on the pulsatile flow field for the physiological flow.*

1. Introduction

Atherosclerosis is a disease of large and medium-sized arteries in which cells, such as macrophages, smooth muscle cells and lipids, accumulate in the intima layer of arteries forming focal lesions or plaques. As a plaque grows with time, it will cause a partial reduction in the arterial cross-sectional area (stenosis). These stenosis, or constriction, has a complex influence on blood flow through and beyond the narrowed segment of artery. The possibility that haemodynamic factors may participate in genesis and proliferation of atherosclerosis has fostered increasing study of flow through arterial stenosis during the past decades. It has been established that the development of advanced atherosclerotic plaques may occur preferentially in high shear regions. It is, therefore, worthwhile from the fluid dynamics point of view to study and identify regions of very high shear and normal stresses in the flow (haemolysis), regions of very low or very high shear stress at walls (atheromatous lesions) and the extent of separated or reversed flow regions (thrombosis) in vascular tubes.

Numerical simulation of arterial stenosis provides an effective means of obtaining detailed flow patterns associated with the disease. One of the first numerical studies on this type of problem was done by Lee and Fung (1970) to study the blood flow in locally constricted tubes for a Reynolds number range of 0-25. A bell-shaped constriction of Gaussian normal distribution curve with a diameter constriction of 50 per cent was used. From then on, haemodynamical

International Journal of Numerical Methods for Heat & Fluid Flow
Vol. 14 No. 5, 2004
pp. 689-713

0961-5539
DOI 10.1108/09615530410539991

characteristics of flow through stenosis have been continually investigated in the past 30 years. Numerical simulation to steady flow through rigid stenoses has been reported by many investigators (Deshpande *et al.,* 1976; Lee, 1990, 1994; Siegel *et al.*, 1994).

For pulsatile flow through stenosis, Back *et al.* (1977) presented a numerical solution to pulsatile flow in the coronary artery of man with double constrictions, assuming a rigid boundary. O'Brien and Ehrlich (1985) numerically studied the pulsatile flow through a constricted artery using a vorticity-streamline formulation and reaffirmed the importance of studying unsteady rather than steady flow. Similarly, Huang *et al.* (1995) simulated both steady and unsteady flow through rigid tube with a smooth stenosis.

Most experimental and numerical studies of pulsatile flow through stenosed arteries have been performed under the assumption of a simple periodic variation of the inflow with time. But evidences show that the arterial flux waves are different from a single harmonic pulse. For the physiological flow, generally, the waveform given by McDonald (1955) for the canine femoral artery is used. Zendehbudi and Moayeri (1999) obtained and compared the flow fields through the constriction of a cosine function for the physiological flow and an equivalent pulsatile flow. Deplano and Siouffi (1999) and Tu *et al.* (1992) gave the numerical simulations for other types of physiological flows that have different velocity profiles, using finite element packages. Tu and Deville (1996) gave a further numerical study on that type of physiological flow by considering the non-Newtonian behaviour.

In the present study, the physiological pulsatile flows in the tube with a bell-shaped stenosis are investigated in detail. In order to have a relatively thorough understanding of the physiological flow, a detailed analysis on the dynamics of the flow over a bell-shaped stenosis for the physiological flow, including the comparison of the physiological and other two pulsatile flows and the effects that some flow parameters put on the flow field in stenosed arteries, is presented in the current study. The problem is solved by using the method which has been developed by Lee *et al.* (2001) to solve the steady and unsteady incompressible Navier-Stokes equations in a two-dimensional, curvilinear coordinate system. The numerical solutions are obtained under the conditions of laminar flow, Newtonian fluid and rigid wall.

2. Governing equations and numerical procedures

2.1 Governing equations

For axially symmetric flow of incompressible Newtonian fluids, the Reynolds-average governing equations of two-dimensional flow can be written in axisymmetric coordinate system as follows:

$$\frac{\partial(ru)}{\partial z} + \frac{\partial(rv)}{\partial r} = 0 \tag{1a}$$

$$\frac{\partial(ru)}{\partial t}+\frac{\partial(ru)^2}{\partial z}+\frac{\partial(ruv)}{\partial r}=-\frac{\partial(rp)}{\partial z}+\frac{\partial}{\partial z}\left(r\gamma\frac{\partial u}{\partial z}\right)+\frac{\partial}{\partial r}\left(r\gamma\frac{\partial u}{\partial r}\right) \quad (1b)$$

$$\frac{\partial(rv)}{\partial t}+\frac{\partial(ruv)}{\partial z}+\frac{\partial(rv)^2}{\partial r}=-\frac{\partial(rp)}{\partial r}+\frac{\partial}{\partial z}\left(r\gamma\frac{\partial v}{\partial z}\right)+\frac{\partial}{\partial r}\left(r\gamma\frac{\partial v}{\partial r}\right)+p-\gamma\frac{v}{r} \quad (1c)$$

Here u and v are the velocity components in z and r directions, respectively.

Chorin (1967) developed the artificial compressibility approach for solving steady incompressible flow. This involved modifying the governing equations to make them fully hyperbolic by adding an unsteady term to the mass conservation equation. The steady-state solution is not altered by modifying the equations in this way. As shown in Lee *et al.* (2001), the artificial compressibility approach has been developed to solve both steady and unsteady flows. In the present study, the artificial compressibility formulation developed by Lee *et al.* (2001) is used to solve pulsatile laminar flows through arterial stenosis. With this method, the pseudo-unsteady terms are added to both mass conservation equation and momentum equations. Then, the non-dimensional governing equations of two-dimensional flow in the conservation form can be expressed in a generalized curvilinear coordinate system with the axisymmetric physical components taken as the dependent variables as follows:

$$\frac{\partial W}{\partial \tau}+K\frac{\partial W}{\partial t}+\frac{\partial E}{\partial \xi}+\frac{\partial F}{\partial \eta}=\frac{\partial E_V}{\partial \xi}+\frac{\partial F_V}{\partial \eta}+S \quad (2)$$

where

$$W=Jr\begin{bmatrix}p\\u\\v\end{bmatrix}$$

$$E=Jr\begin{bmatrix}\beta U\\uU+p\xi_z\\vU+p\xi_r\end{bmatrix}\quad F=Jr\begin{bmatrix}\beta V\\uV+p\eta_z\\vV+p\eta_r\end{bmatrix}$$

$$E_v=Jr\frac{1}{\mathrm{Re}}\begin{bmatrix}0\\\alpha_1u_\xi+\alpha_2u_\eta\\\alpha_1v_\xi+\alpha_2v_\eta\end{bmatrix}\quad F_v=Jr\frac{1}{\mathrm{Re}}\begin{bmatrix}0\\\alpha_2u_\xi+\alpha_3u_\eta\\\alpha_2u_\xi+\alpha_3v_\eta\end{bmatrix}$$

$$S = Jr \begin{bmatrix} 0 \\ 0 \\ \frac{p}{r} - \frac{1}{\mathrm{Re}} \frac{v}{r^2} \end{bmatrix}$$

$$K = \mathrm{St} \begin{bmatrix} 0 & 0 & 0 \\ 0 & 1 & 0 \\ 0 & 0 & 1 \end{bmatrix} \quad \text{(for unsteady flow)}$$

$$K = 0 \quad \text{(for steady flow)}$$

In the governing equations, τ is a pseudotime variable and t is the physical time. β is an artificial compressibility parameter. The dimensionless variables $r^* = r/r_0$, $z^* = z/r_0$, $u^* = u/u_0$, $v^* = v/u_0$, $t^* = t/t_0$ and $p^* = p/\rho u_0^2$ have been used and asterisks are dropped for brevity. $\mathrm{St} = r_0/(u_0 t_0)$ and $\mathrm{Re} = r_0 u_0/\gamma$ are the Strouhal and Reynolds numbers, respectively. Generally, t_0 is taken as $1/\varphi$ for a pulsatile flow on the assumption that φ is the angular frequency of the pulsatile flow. Here, J is the Jacobian of the transformation. U and V are contravariant velocities in ξ, η-direction is given by

$$U = \xi_z u + \xi_r v$$

$$V = \eta_z u + \eta_r v$$

and

$$\alpha_1 = \xi_z^2 + \xi_r^2, \quad \alpha_2 = \xi_z \eta_z + \xi_r \eta_r, \quad \alpha_3 = \eta_z^2 + \eta_r^2$$

In deriving the equations, constant density and constant viscosity is assumed for simplicity. As shown above, the system of governing equations can be used to describe both steady and unsteady flows. A solution of the modified equations that is steady in pseudotime is identical to the instantaneous unsteady solution of the governing equations.

2.2 Numerical procedures

The governing equations are discretized using a cell-centered finite volume method. To allow the selection of the pseudotime step $\Delta\tau$ without regard to stability restriction, an implicit pseudotime discretization is used for equation (2). At the same time, the physical time-accurate term in equation (2) is discretized in an implicit fashion by means of a second-order-accurate, three-point backwards difference in physical time. So a prototype implicit scheme for equation (2) can be formulated as

$$\frac{W^{n+1,m+1}-W^{n+1,m}}{\Delta\tau}+K\frac{1}{2\Delta t}[3W^{n+1,m+1}-4W^{n}+W^{n-1}]$$
$$+\theta\left(\frac{\partial E}{\partial\xi}+\frac{\partial F}{\partial\eta}\right)^{n+1,m+1}+(1-\theta)\left(\frac{\partial E}{\partial\xi}+\frac{\partial F}{\partial\eta}\right)^{n+1,m}=\left(\frac{\partial E_V}{\partial\xi}+\frac{\partial F_V}{\partial\eta}\right)^{n+1,m}+S^{n+1,m} \quad (3)$$

where superscripts m and n are mean pseudotime and physical time, respectively.

The Lower-Upper Symmetric-Gauss-Seidel (LU-SGS) implicit algorithm is used as the time integration scheme for the governing equations because of its efficiency and stability. When constructing this scheme, the advantages of recent advances in computational fluid dynamics are considered. The LU-SGS method is applied with the use of upwind-biased and total variation diminishing (TVD) scheme. To calculate the convective flux, an edge-based method is used by calculating and storing the flux integrals based on the edges. The convective fluxes are discretized by using the appropriate form of Roe's flux-difference splitting (Lee *et al.*, 2001; Roe, 1981). The viscous terms are evaluated by a Gauss integration in the finite volume method way, resulting in a second-order central differencing.

High order accuracy is obtained using Monotonic Upstream Schemes for Conservation Laws MUSCL scheme (Hirsch, 1990), which is a nominally higher order upwind-biased extrapolation scheme. The left and right state vectors W_{L} and W_{R} at a control volume surface of an edge $i+1/2$ can be evaluated using MUSCL scheme. In order to obtain solutions satisfying TVD conditions for suppressing excessive non-physical oscillations and ensuring the numerical stability, functions of the flux limiter are introduced.

The details of the current numerical method for incompressible laminar flows can be found in Lee *et al.* (2001). The artificial compressibility parameter β influences both stability and efficiency in the numerical computation. As has been referred to in Lee *et al.* (2001), the current scheme is found not to be sensitive to the value of the artificial compressibility parameter and the present code is stable for a wide range of β. In the present study, a constant value of the parameter β has been used. For all cases, the value of β that is set to 10 is found to give a good rate of convergence and accuracy for all of the problems considered.

3. Geometry configuration and boundary conditions

The geometrical configuration of the vascular tube with a stenosis and its coordinate system is shown in Figure 1. The coordinate variables (r, z) are defined in the cylinder coordinate system; r_0 is the radius of the tube having a constant cross section; d_{c} is the opening of the constriction; and L is the length of the tube under consideration.

The geometry of the stenosis may be described by the following bell-shaped Gaussian distribution profile

$$f(z) = 1 - c\exp(-c_s z^2) \tag{4}$$

where c is the constriction ratio and is equal to $(D - d_c)/D$ and c_s is a shape constant. In the present study, c_s is fixed at 4.0.

In this work, boundary conditions are imposed using halo cells that are two rows of fictitious cells next to the boundary. With this concept the boundary fluxes can be treated in a fashion similar to the internal fluxes. At the inflow boundary, the velocities are specified and the pressure is extrapolated from the interior. For internal flows at the outflow boundary the velocities are extrapolated from the interior and a constant static pressure is imposed. On a solid surface, the usual no-slip condition is applied. The pressure at the wall is obtained by setting the gradient of the pressure equal to zero at the no-slip wall.

The average inlet velocity is specified according to the three types of pulsatile flows as shown in Figure 2. Type I – physiological flow, $u(t)$ is the same as that given by other authors (McDonald, 1955); Type II – equivalent pulsatile flow, $u(t) = 1 - \alpha[1 + \cos(t + \delta)]$; Type III – simple pulsatile flow, i.e. pure sinusoidal flow, $u(t) = \sin(t)$. The physiological flow is selected due to its direct

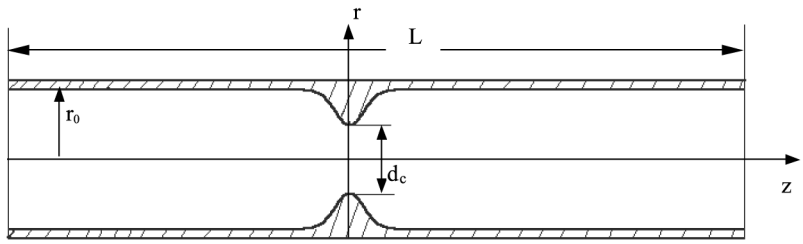

Figure 1.
The geometry of the bell-shaped stenosis

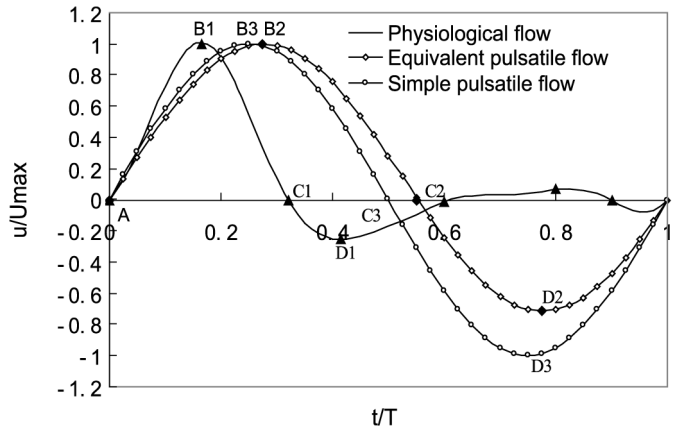

Figure 2.
Time variation of the velocity for the physiological, equivalent pulsatile and simple pulsatile flows

relevance with the investigation of intracardiac flow, blood vessel stenosis and heart valvular regurgitation. The sinusoidal flow is often used in the initial studies for pulsatile blood flow and many other engineering applications. The equivalent pulsatile flow was first used by Zendehbudi and Moayeri (1999). The equivalent pulsatile flow profile is hoped to have the same stroke volume as the physiological flow profile. After integrating, the equivalent pulsatile flow can be obtained by setting $\alpha = 0.858$ and $\delta = 1.405$. In Figure 2, t is non-dimensional physical time and T is the period of the pulsatile flows.

In the present study, the dimensionless Reynolds, Strouhal and Womersley numbers are defined, respectively, as

$$\mathrm{Re} = \frac{u_0 r_0}{\gamma}$$

$$\mathrm{Wo} = r_0 \sqrt{\frac{\varphi}{\gamma}} \tag{5}$$

$$\mathrm{St} = \frac{\mathrm{Wo}^2}{\mathrm{Re}} = \frac{r_0 \varphi}{u_0}$$

where r_0 is the radius of the tube infinitely far upstream where the section becomes uniform; u_0 is the maximum value, in the period, of the average velocity over the section of inlet; and φ is the angular frequency of the pulsatile flow. The Womersley number is an indication of the main frequency of the flow. In physiological situations, the frequency of the flow is determined by the heart rate. For the physiological flow in a femoral artery of dog, the pulsatile flow characteristics were obtained from MacDonald's measurements (Daly, 1976; McDonald, 1955). The frequency parameter Wo is about 3.34 while the peak Reynolds number is about 400. So the basic Reynolds and Womersley numbers used in the present study are set to 400 and 3.34, respectively. A large number of computations are conducted in this work for different combinations of the Reynolds and Womersley numbers and constriction ratio.

4. Further validation of computational results

In our earlier study (Lee *et al.*, 2001), a variety of computed results have been presented to validate the present numerical method and computer code. Here two other test cases based on constricted circular tubes are considered for further validation.

4.1 Steady laminar flow in a circular tube with a stenosis for Re=200

In this case, the steady laminar flow in a tube with a stenosis is predicted. The geometry of the stenosis may be described by the following profile:

$$\frac{r}{r_0} = 1 - \frac{\delta}{2r_0}\left(1 + \cos\frac{\pi z}{z_0}\right), \quad -z_0 \le z \le z_0 \tag{6}$$

In this case, $\delta = 1/2$, and $z_0 = 1.0$. The computation is done with a 201×41 grid. Figure 3 shows the axial velocity profiles at different axial positions for $\mathrm{Re} = 200$ in comparison with the computational data obtained by Deshpande *et al.* (1976). Here the Reynolds number is based on the maximum upstream velocity. As shown in Figure 3, these velocity profiles fit the numerical results of Deshpande *et al.* (1976) very well.

4.2 Simple pulsatile laminar flow inside a circular tube with a stenosis

This case deals with the simple pulsatile laminar flow inside a circular tube with a stenosis. In this case, the geometry of the stenosis is specified by equation (6) with $\delta = 1/4$, and $z_0 = 1.0$. A simple sinusoidal pulsatile velocity is added in the inlet

$$U(t) = 1 + \sin(t)$$

with $\mathrm{Re} = 50$, and $\mathrm{Wo} = 10$. Here t is the non-dimensional physical time.

The instantaneous streamlines during one cycle for the simple sinusoidal pulsatile flow are shown in Figure 4 at every eighth of a cycle. The current results can be compared with those of Huang *et al.* (1995, Figure 6) at the same physical time instants. For this stenosis model, there is no separation in the steady state at $\mathrm{Re} = 50$. So it can be found that in the unsteady flow the flow fields are greatly different from those in steady flow. There is no separation in the first quarter of one cycle, even at $t = 0.25\,\mathrm{T}$ when the flow reaches peak forward value. At $t = 0.375\,\mathrm{T}$, a small vortex occurs behind the stenosis. Then the vortex develops rapidly and there is a large recirculation region distal to the stenosis while the separation also appears in the upstream near the stenosis. Until $t = 0.75$ when the flow has zero flux, the recirculation flow occupies most of the tube volume. Then the vortices begin to weaken. By the end of one cycle, the vortices disappear and another cycle starts again.

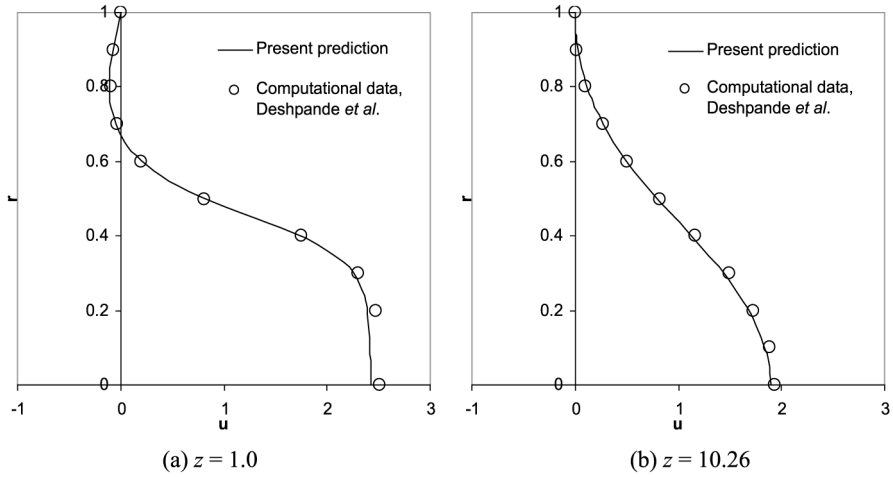

Figure 3.
A comparison of the present prediction and the computational data of Deshpande *et al.* (1976) for axial velocity profiles at different axial positions

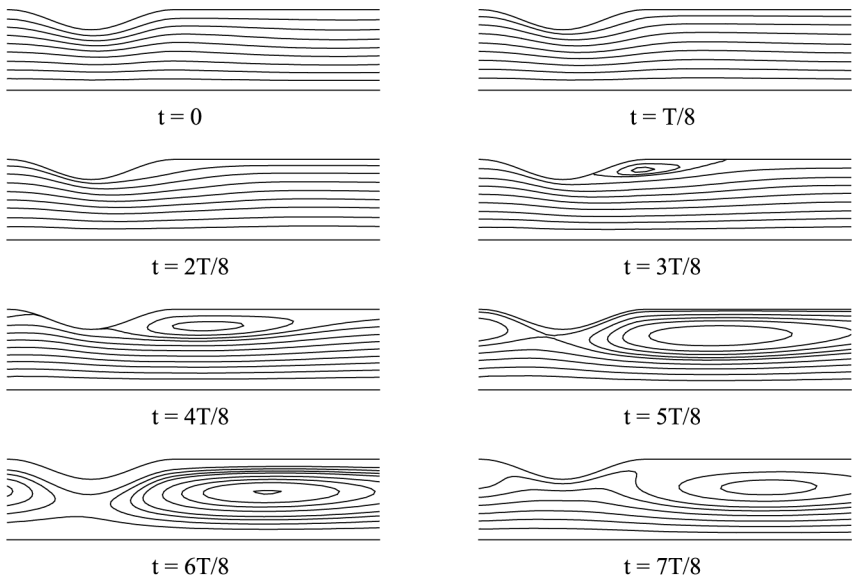

Figure 4.
The instantaneous streamlines in one cycle for the flow at Re = 50, and Wo = 10

The development process of the separation described above is verified by Huang *et al.* (1995) too. The comparison between the two numerical solutions shows a very good agreement.

5. Results and analysis

In the present study, the pulsatile laminar flows in the tube with a bell-shaped stenosis are investigated in detail. The computational domain is taken as 26 radii. A non-uniform grid, which is stretched in the height direction, is used in the present computation. Grid independence tests show that a grid size of 181×35 $(z \times r)$ is sufficient for the present range of flow investigation. The (crude) computational grid in the stenosed region is shown in Figure 5. The number of time steps per cycle is taken to be 80, which corresponds to a non-dimensional real-time step $\Delta t = 2\pi/80$. For all cases in this study, the flow characteristics are presented only at some selected instants. The selected instants involve four points corresponding to the conditions of initial zero, peak forward, middle zero and peak backward flow rates, on each waveform, i.e. at the points A, B ($B1$, $B2$, $B3$), C ($C1$, $C2$, $C3$) and D ($D1$, $D2$, $D3$) as shown in Figure 2. For the physiological flow, A, B, C and D correspond to the instants 0, 0.165, 0.32 and 0.415 T. For the equivalent pulsatile flow, A, B, C and D

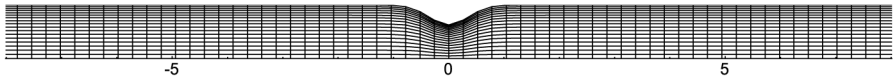

Figure 5.

Note: The (crude) computational grid in the stenosed region

correspond to 0, 0.275, 0.55 and 0.775 T. For the simple pulsatile flow, *A*, *B*, *C* and *D* is 0, 0.25, 0.5 and 0.75 T, respectively. It can be noticed that for the physiological flow, at the instants 0, 0.32, 0.6 and 0.9 T, the net flow rates are zero or near zero.

5.1 Comparison of numerical results for the three types of pulsatile flows

The numerical results of all three types of pulsatile flows are illustrated here for the case of Re = 400, Wo = 3.34, and $c = 0.375$. The flow field developments of the physiological, equivalent and simple pulsatile flow are shown in Figures 6-8. As shown in these figures, the recirculation zones occupy both distal and proximal region; to the stenosis when the net inlet flow is zero or near zero. The distribution of the vortices in other time levels looks analogous to that in steady flow. For the physiological flow, the zero flow rate occurs four

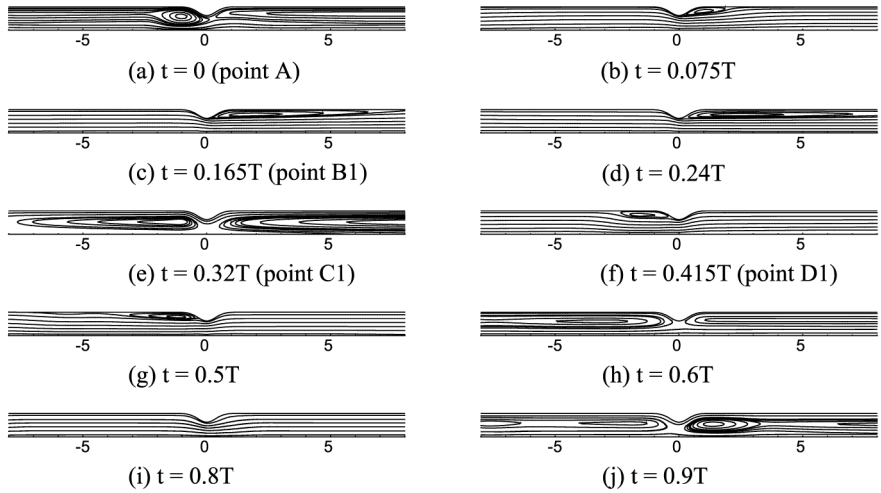

Figure 6.
The instantaneous streamlines in the tube with a stenosis for the physiological flow

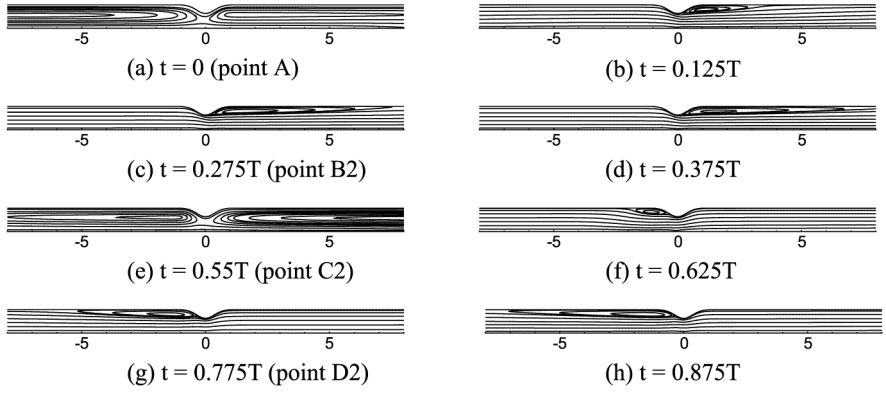

Figure 7.
The instantaneous streamlines in the tube with a stenosis for the equivalent pulsatile flow

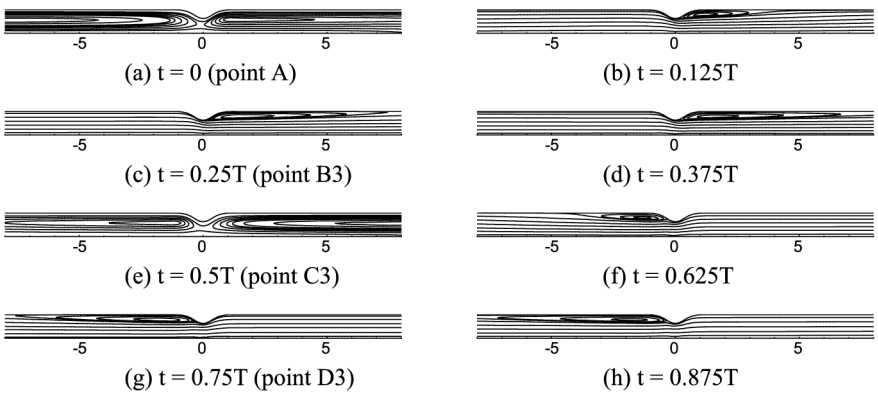

Figure 8.
The instantaneous streamlines in the tube with a stenosis for the simple pulsatile flow

times in one cycle while the zero net flow occurs only twice in the same cycle for the other two flows. So the time during which the large recirculation zones fill most of the flow field for the physiological flow is much longer than that for the other two pulsatile flows in one cycle. It can be found that for the simple pulsatile flow, the flow field development in the first half cycle is symmetric with that in the second half cycle with respect to the stenosis. This is because the simple pulsatile inflow has a velocity waveform that is reversely symmetric between its first and second half cycles. The flow development of the equivalent flow is similar to that of the simple pulsatile flow because of similar inlet velocity profiles except that the recirculation zones for the equivalent flow are smaller than those for the simple pulsatile flow at the corresponding instants during the second half cycle. This is due to the fact that the magnitude of the peak backward flow rate for the equivalent pulsatile flow is only about three-fourth of that for the simple pulsatile flow.

The mean velocity fields for the three pulsatile flows are shown in Figure 9. The mean quantity is computed by averaging over a cycle after a stationary state was reached. As shown in Figure 9(c), for the simple pulsatile flow, the mean streamline contours are symmetrical with respect to the stenosis because of the symmetrical behaviour of the sinusoidal profile. The flow zones with the large recirculating vortices exist in both sides of the stenosis. From Figure 9(b), it can be seen that for the equivalent pulsatile flow, there exists the strong vortex in the distal end of the stenosis while the curving streamlines in the proximal end of the stenosis are evidently caused by the vortices formed in some instants. This is because the forward flow rate is higher than the backward flow rate during one cycle for the equivalent pulsatile flow. In contrast, for the physiological flow, the flow zone with large separation occurs only in the region distal to the stenosis as seen in Figure 9(a) because its forward flow rate predominates over the backward flow rate during one cycle.

The non-dimensional wall vorticity is of physiological importance since it is proportional to wall shear stress that is often employed as indicator functions

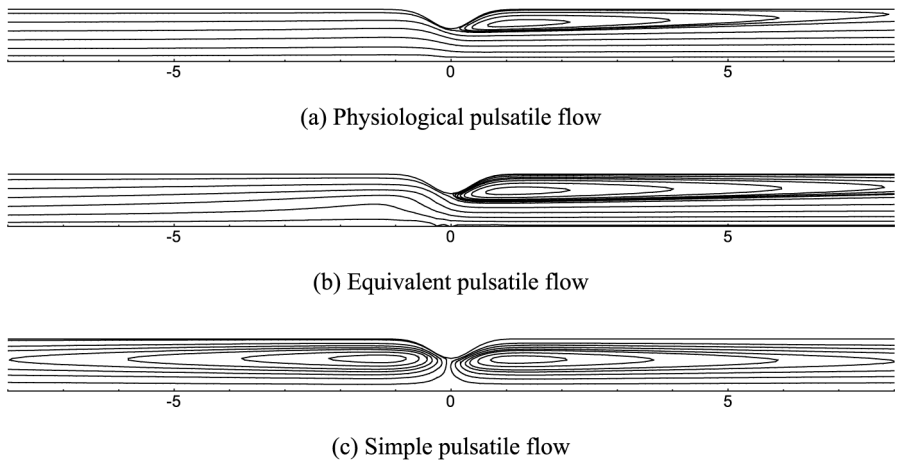

Figure 9.
The mean flow characteristics by averaging in time over one cycle for the three pulsatile flows

for the onset and development of arterial diseases. The instantaneous wall vorticity distributions at the points *A*, *B*, *C* and *D* for the three pulsatile flows are shown in Figure 10. It can be seen that the wall vorticity grows up rapidly and reaches its peak value in the vicinity of the stenosis. For each pulsatile flow, the magnitudes of the peak wall vorticity near the stenosis at the points *B*

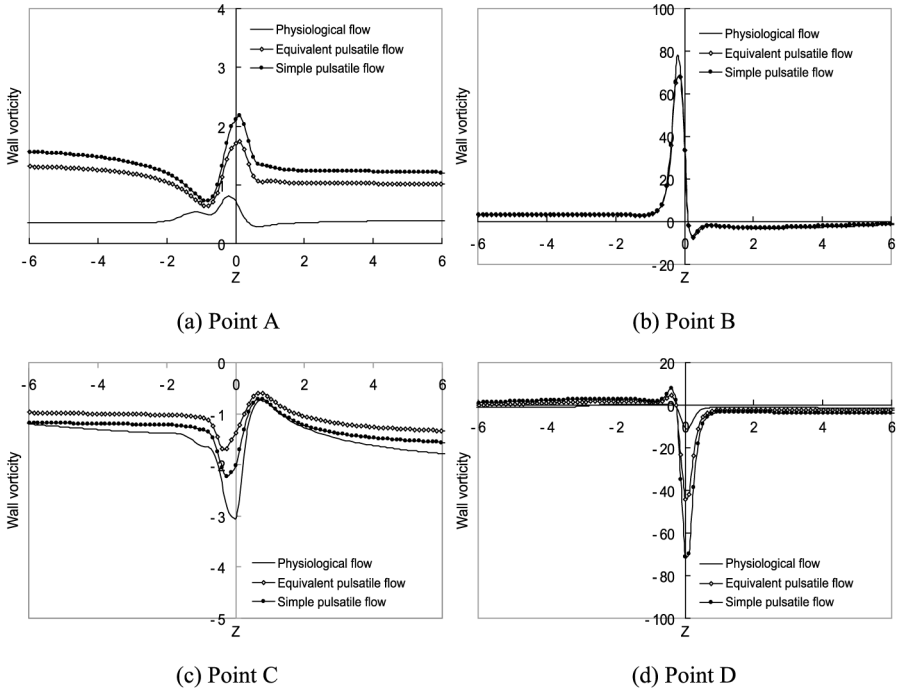

Figure 10.
The comparison of the instantaneous wall vorticity distributions at the points *A*, *B*, *C* and *D* for the three pulsatile flows

and D are always much higher than the corresponding ones at the points A and C. Evidently, the greater instantaneous flow rate leads to higher peak wall vorticity for the three pulsatile flows. So we should pay main attention to examining the flow behavior at the points B and D. The distributions of wall vorticity for the three pulsatile flows are almost the same at point B where their flow rates are also the same and reach the positive peak value. In contrast, this is not the case for the point D. The largest peak value of wall vorticity at the point D occurs for the simple pulsatile flow and the smallest one for the physiological pulsatile flow. This is due to the fact that the magnitude of the backward flow rate for the physiological flow is just about one-third or one-fourth as large as that for the equivalent pulsatile flow or that for the simple pulsatile flow, respectively.

The time-averaged wall vorticity in one cycle for the three pulsatile flows are shown in Figure 11(a). It can be seen that the equivalent and simple pulsatile flows have almost the same positive peak mean wall vorticity while the positive peak mean wall vorticity for the physiological flow is nearly one half as large as those for these two pulsatile flows. At the same time, the largest negative mean wall vorticity occurs for the simple pulsatile flow while the smallest one appears for the physiological flow. Figure 11(b) shows the maximum instantaneous wall vorticity distribution which is composed of the instantaneous wall vorticity with the maximum absolute value in the whole cycle at every position along the wall. It can be found that the positive peak wall vorticity for the physiological flow is a bit higher than those in the other two pulsatile flows. But the differences between them are very small. The negative peak maximum wall vorticity distribution has similar trend to negative peak mean wall vorticity distribution. So it can be concluded that the peak value and variation range (maximum minus minimum) of wall vorticity will be overestimated if the equivalent or simple pulsatile inflow is used instead of the actual physiological one in the study of the arterial flow through stenosis.

At the points B and D, there exists the peak flow rates which put more distinguished impact on the flow field developments than the zero flow rates at the points A and C. So only the instantaneous wall pressure

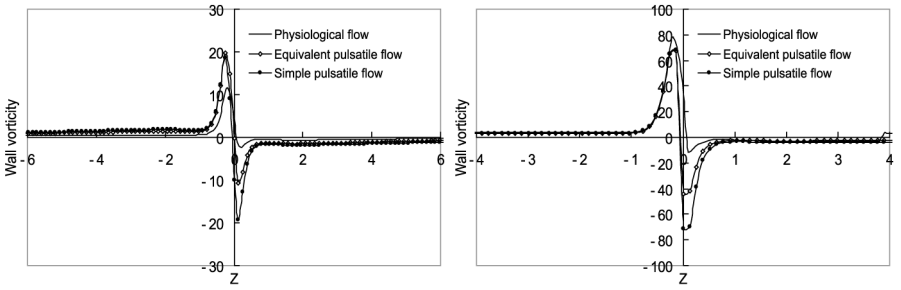

(a) Time-average wall vorticity (b) Maximum instantaneous wall vorticity

Figure 11.
The wall vorticity distribution in one cycle for the physiological, equivalent flow and simple pulsatile flows

distributions at the points *B* and *D* for the three pulsatile flows are shown in Figure 12. The pressures at both points *A* and *C* (not shown here) almost linearly change (decrease or increase) along the tube wall. In contrast, at the points *B* and *D*, the flow has a large pressure drop in the passing the stenosis and pressure recovers partially in the downstream region of the stenosis in the flow direction. At the point *B*, the variation of wall pressures along the wall has almost the same trend for the three pulsatile flows while at the point *D*, the largest wall pressure drop occurs for the simple pulsatile flow and the smallest for the physiological flow. The wall pressure drop for the physiological flow is much less than those for the other two pulsatile flows at the point *D*.

This centerline velocity is also an important parameter in the study of pulsatile flow fields. The distributions of velocity along the centerline for the three pulsatile flows are shown in Figure 13 at the points *B* and *D*. From this figure, it can be found that for the three pulsatile flows, the peak centerline velocity at the points *B* and *D* all occurs at a position slightly downstream of the throat in the inflow direction. At the point *B*, the distributions of the centerline velocity are the same for the three pulsatile flows and the velocity recovers very slowly after passing through the stenosis. This illustrates that

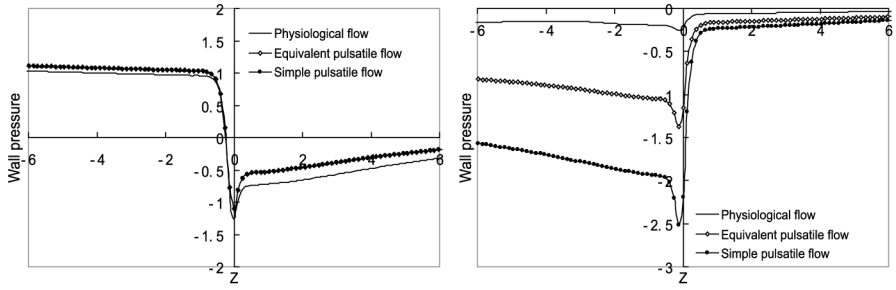

Figure 12.
The comparison of the instantaneous wall pressure distributions at the points *B* and *D* for the three pulsatile flows

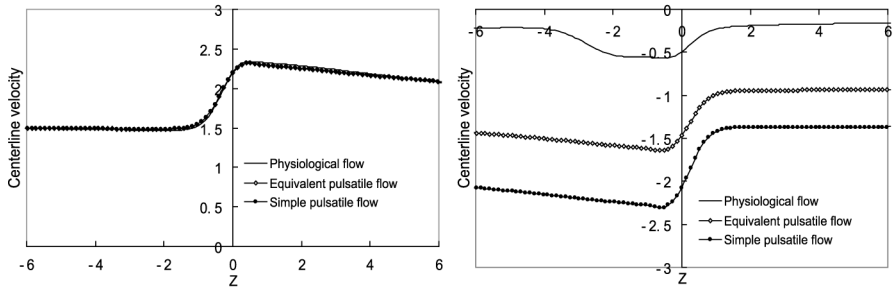

Figure 13.
The comparison of the instantaneous centerline velocity distributions at the points *B* and *D* for the three pulsatile flows

a large recirculation zone exists behind the stenosis and leads to the decrease of the actual flow section. At the point D, the largest magnitude of peak centerline velocity occurs for the simple pulsatile flow and the smallest for the physiological flow. Actually, the characteristics of the centerline velocity distribution are tightly related to the flow rate and the distribution of the recirculating vortices in the instantaneous flow fields for the pulsatile flows.

According to the above discussion, the flow characteristics of the physiological flow have distinct differences from those of the other two pulsatile flows while the flow patterns of the other two flows are similar to each other. At the instants where the net flow rate is zero, the recirculation zones always prefer to simultaneously occur both proximal and distal to the stenosis for these pulsatile flows. For the physiological flow, therefore, the large recirculation zones that fill most of flow field appear more frequently. It can be found that the flow field characteristics of the three pulsatile flows are very similar at the peak forward flow rate. At the peak backward flow rate, however, the magnitudes of negative peak values of the flow variables examined here for the physiological flow are always much less than those for the other two pulsatile flows. Furthermore, the peak values and variation range of mean and instantaneous wall vorticity for the equivalent and simple pulsatile flows are larger than those for the physiological flow. So the flow characteristics cannot be properly estimated if the equivalent or simple pulsatile inlet flow is used in the study of pulsatile arterial flow through stenosis instead of the actual physiological one.

5.2 Numerical research for the physiological pulsatile flow

In order to have a deeper understanding of the physiological flow, we further consider the effects that the constriction ratio, Womersley number and Reynolds number put on the flow fields. Here the physiological flow at $\mathrm{Re} = 400$, $\mathrm{Wo} = 3.34$ and $c = 0.375$ is considered as a basic case which has been discussed above.

5.2.1 The effect of constriction ratio. It is well known that the constriction ratio has a great influence on the flow field through the stenosed artery for steady flow. In the present study, how the characteristics of the flow vary with the variation of constriction ratios are discussed for the physiological flow. Other two constriction ratios $c = 0.5$ and 0.6 are considered here with the same Reynolds and Womersley numbers as those in the basic case. The flow developments for the constriction ratios $c = 0.5$ and 0.6 have no significant differences from that for $c = 0.375$. So only streamline contours for $c = 0.5$ are shown in Figure 14. It can be found that flow development for $c = 0.5$ is very similar to that for $c = 0.375$. With increasing constriction ratio, however, the corresponding recirculation zone in the flow field becomes larger and stronger.

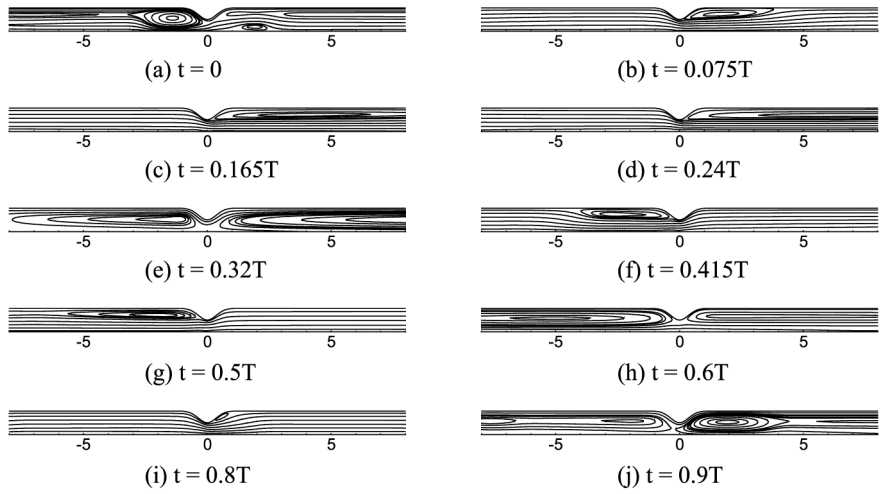

Figure 14.
The instantaneous streamlines in the tube with a stenosis for the physiological flow with the constriction ratio $c = 0.5$

The time-averaged wall vorticity and maximum instantaneous wall vorticity distributions in one cycle for $c = 0.375$, 0.5 and 0.6 are shown in Figure 15. From Figure 15, we can find that whether for mean wall vorticity or maximum instantaneous wall vorticity, the largest value and variation range in one cycle depend monotonically on the constriction ratio c. The peak value of wall vorticity increases dramatically with the increasing constriction ratio. The constriction ratios $c = 0.375$, 0.5 and 0.6 correspond to the 61, 75 and 84 per cent area reduction, respectively. Although the differences of area reduction caused by different constriction ratios are not so large, the peak value of wall vorticity for $c = 0.6$ is more than four times higher than that for $c = 0.375$ and two times higher than that for $c = 0.5$. So the severe stenosis can lead to the rapid growth of the peak wall vorticity, which is very similar to the situation in steady flow.

The general nature of the pressure field can be suggested by its variation along the centerline of the artery. Figure 16 shows the variations of centerline

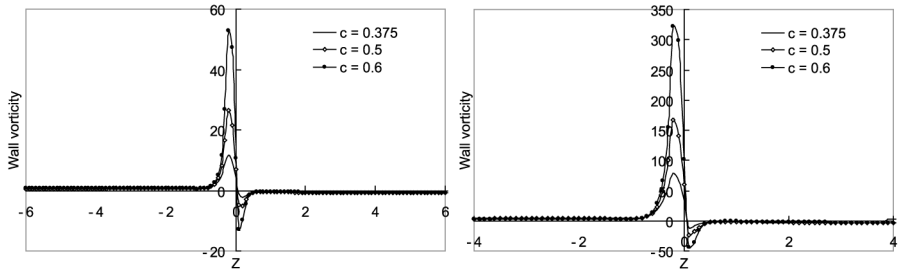

Figure 15.
The wall vorticity distribution in one cycle at different constriction ratios for the physiological flow

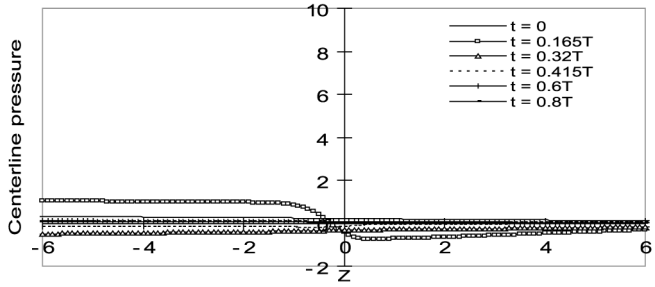

(a) $c = 0.375$

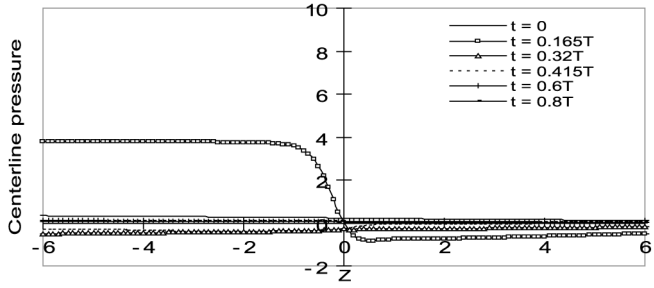

(b) $c = 0.5$

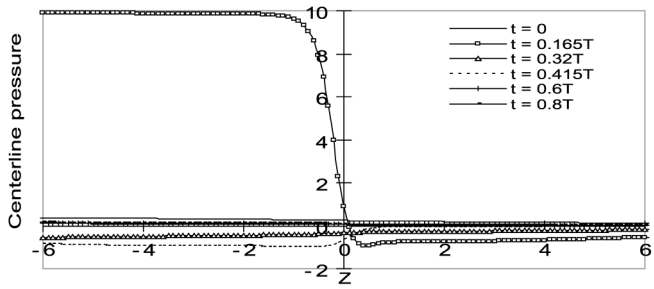

(c) $c = 0.6$

Figure 16.
The instantaneous centerline pressure distribution at different constriction ratios for the physiological flow

pressure for the three constriction ratios at different instants in one cycle. As shown in Figure 16(a)-(c), for all the three constriction ratios, the variation of pressure at $t = 0.165$ T is the largest among all the selected instants because of the largest flow rate. At this instant, the pressure decreases greatly through the stenosis and recovers partially downstream of the stenosis. It can be seen that more severe stenosis leads to a larger pressure drop through the stenosis. At almost all instants, the pressure varies in a greater range for the more severe stenosis.

According to the above analysis, the constriction ratio contributes distinct effect on the flow field for the physiological flow. In general, the severe stenosis

can lead to great recirculation zones in the flow fields and cause the flow variables considered here, such as peak wall vorticity and centerline pressure drop, to increase dramatically.

5.2.2 The effect of Womersley number. In order to study the effect of varying Wo, the physiological flows for the Womersley numbers from 0 to 10 with the same Reynolds number and constriction ratio are considered here. In this study, the flow fields for Wo = 2 and 6 with the same Re = 400, and $c = 0.375$ are shown in Figure 17(a) and (b), respectively. By comparing the streamlines at the corresponding time level in Figures 17 and 6, we can find that the flow patterns for Wo = 2 are very similar to those for Wo = 3.34 except that the vortex for Wo = 3.34 is a bit shorter than that for Wo = 2 at the corresponding instant. In contrast, the flow patterns for Wo = 6 are greatly different from those for Wo = 2 and 3.34. During systole, the flow patterns for Wo = 6 are also similar to those for Wo = 3.34. However, the vortex for Wo = 6 is much shorter than that for Wo = 3.34 at the same instant, such as the instant 0.075 and 0.165 T. More significant differences between them are found during diastole. At $t = 0.415$ and 0.6 T, the flow fields for Wo = 6 are more complex and there are more attached vortices to form in comparison with those for Wo = 2 and 3.34. At $t = 0.8$ T, a vortex appears proximal to stenosis for

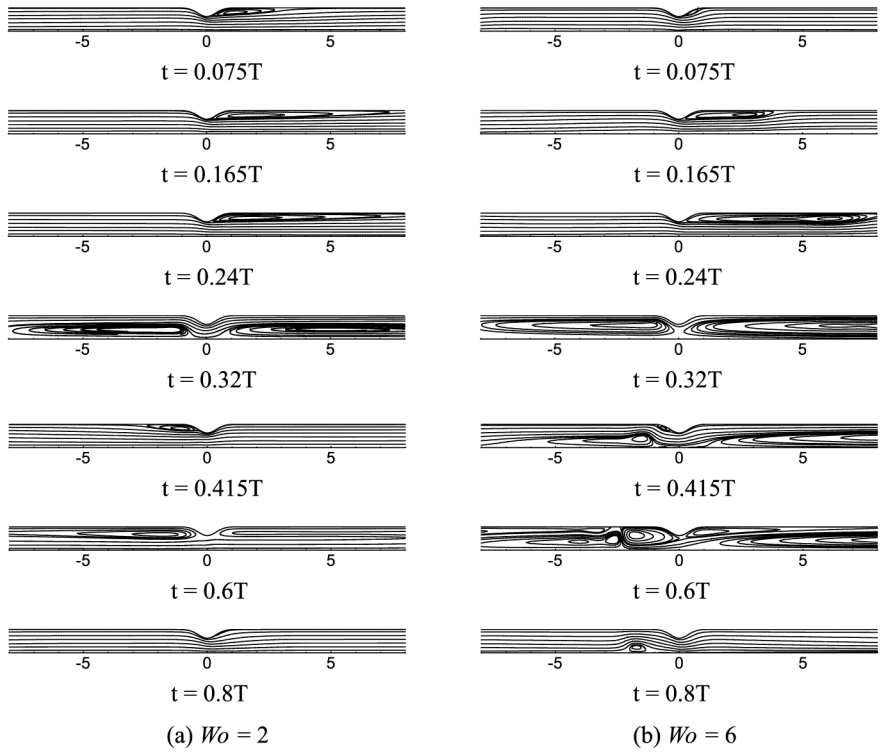

Figure 17.
The instantaneous streamlines in the tube with a stenosis at different Womersley numbers for the physiological flow

Wo = 6 while the streamlines run quite smoothly in the whole flow field for Wo = 2 and 3.34.

The variation in the time-averaged wall vorticity and maximum instantaneous wall vorticity distributions in one cycle is shown in Figure 18. The wall vorticity distribution of a quasi-unsteady flow (Wo = 0) for the same Reynolds number is also shown in Figure 18 together with those for the other three Womersley numbers. The pulsatile flow patterns for a quasi-unsteady flow are the same as those in the steady flow at the same instantaneous Reynolds numbers. As shown in Figure 18, whether for mean wall vorticity distribution or for maximum instantaneous wall vorticity distribution, the largest value and variation range in one cycle slightly increase with the increasing Womersley number. But the differences are very small. As a whole, the distributions of wall vorticity are not significantly affected by the variation of the Womersley number.

The pressure data are treated again and shown in Figure 19. From Figures 16(a) and 19(a) and (b) it can be seen that the developments of centerline pressure distribution have similar trend for different Womersley numbers. The variation of centerline pressure through the stenosis reaches the largest value at $t = 0.165\,\mathrm{T}$ for each Womersley number. At the same time, the pressure drop through the stenosis at $t = 0.165\,\mathrm{T}$ increases slightly with the increase in Womersley number. Besides, it can be found that at most instants, the pressure values vary in a greater range with the increasing Womersley number.

During systole, the blood is pumped out of the heart with forward flow rate. The magnitude of the flow rate during systole is much greater than that during diastole and the forward flow rate predominates in the periodic development of the flow field. Hence, the variations of the reattachment length during systole for the Womersley numbers from 0 to 10 with the Reynolds number 400 are shown in Figure 20. In cases of multiple vortices, the one considered is that closest to the stenosis. In the low Wo-range, such as Wo = 0.6 and 1 in Figure 20(a), the vortex oscillates back and forth during the systole

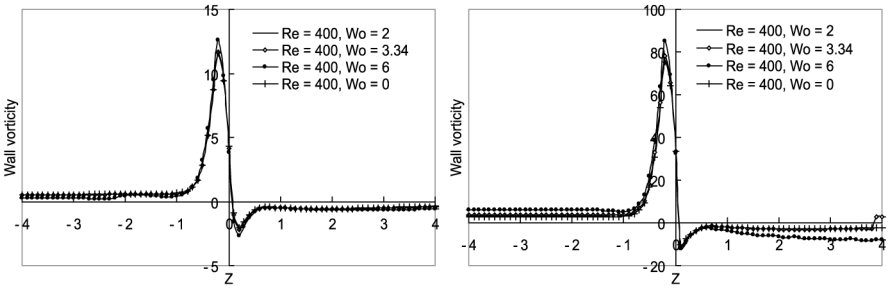

(a) Time-average wall vorticity (b) Maximum instantaneous wall vorticity

Figure 18.
The wall vorticity distribution in one cycle at different Womersley numbers for the physiological flow

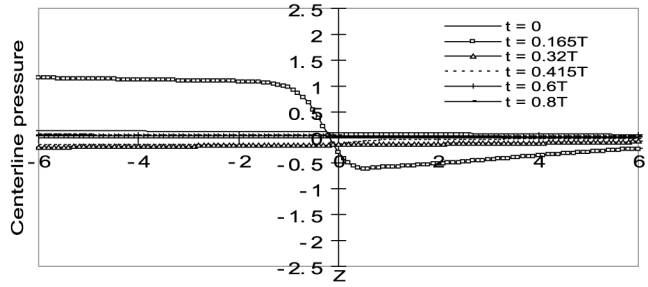

(a) $Wo = 2$

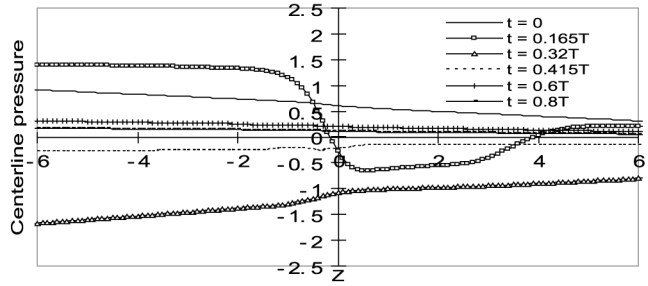

(b) $Wo = 6$

Figure 19.
The instantaneous centerline pressure distribution at different Womersley numbers for the physiological flow

and remains attached to the stenosis. The inertia acquired by the vortex is not sufficient to detach it. In this range, the pulsatile flow resembles steady flow and the pulsatile flow patterns are comparable to those in the quasi-unsteady flow (i.e. when Wo = 0). However, the variations of the reattachment length for Wo = 0.6 and 1 are a bit out of phase with that for the quasi-unsteady flow. Figure 20(b) shows that the variations of the reattachment length in the relatively high Wo-range (with Wo > 2). In this range, the vortex grows up rapidly without oscillating during systole and is washed out from the downstream end. So during the final phase of the systole, the reattachment length is not detectable. In this Wo-range, the growth of the reattachment length is slower for the higher Womersley number. Furthermore, at the same instant, the reattachment length reduces with the increasing Womersley number. It can be found that during the deceleration phase, the vortex can continue to grow up in size and move downstream. Therefore, the flow deceleration is an important factor in vortex formation and translation for the comparatively high Womersley number. Figure 20(b) also shows that the inception time of the vortex is strongly dependent on the values of the Womersley number. The vortex inception time is later for the higher Womersley number.

So it can be concluded that the frequency number Wo has evident effects on the unsteady flow fields. The larger Womersley number will make the flow

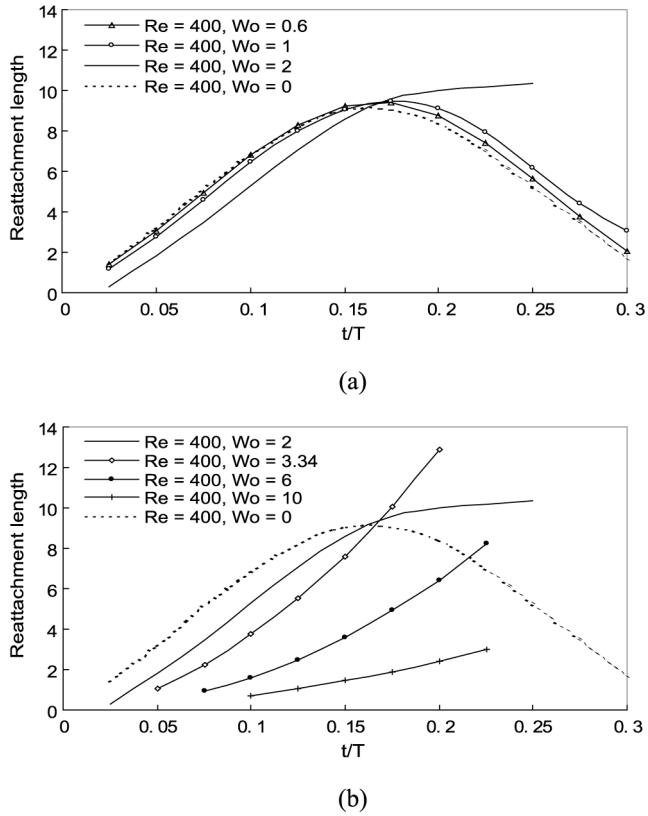

Figure 20.
The reattachment length during systole at different Womersley numbers for the physiological flow

field more complex and cause flow variables to vary in a greater range. Totally, however, the distribution of wall vorticity is not significantly affected. The vortex development in the physiological flow field is strongly dependent on the variation of the Womersley number. At the corresponding instant during systole, the reattachment length reduces with the increasing Womersley number. During the deceleration phase of the systole, the vortex can continue to grow in size and move downstream for the comparatively high Womersley number.

5.2.3 The effect of Reynolds number. The Reynolds number has a great influence on the flow field in the stenosed tube for a steady flow. The effect of the Reynolds number on the physiological pulsatile flow is discussed here. The Reynolds numbers 100, 200 and 400 are considered here with the Womersley number and constriction ratio fixed to 3.34 and 0.375, respectively. Figure 21 shows the details of the flow fields for Re = 200. Although the flow field developments for the Reynolds numbers 100 and 200 seem similar to those for the Reynolds number 400, the variation of Reynolds number still puts great impact on the flow patterns of the physiological flow. Comparing Figure 21

with Figure 6, it can be seen that the recirculation zones proximal to the stenosis only appear together with the recirculation zones distal to the stenosis at the instants when the net flow rates approach zero. At other instants, the strength and size of the vortex caused by stenosis increase with the increasing Reynolds number.

The mean streamline contours for the Re = 100, 200 and 400 are shown in Figure 22(a)-(c), respectively. Referring to Figure 22, a circulation zone is formed behind the stenosis for all the three Reynolds numbers and the vortex length increases with increasing Reynolds number, which is consistent with the characteristics of the steady flow.

The time-averaged and maximum instantaneous wall vorticity distributions in one cycle for Re = 100, 200 and 400 are displayed in Figure 23. For the two computed wall vorticity distributions, the peak value and the variation range of wall vorticity evidently grow with the increasing Reynolds number.

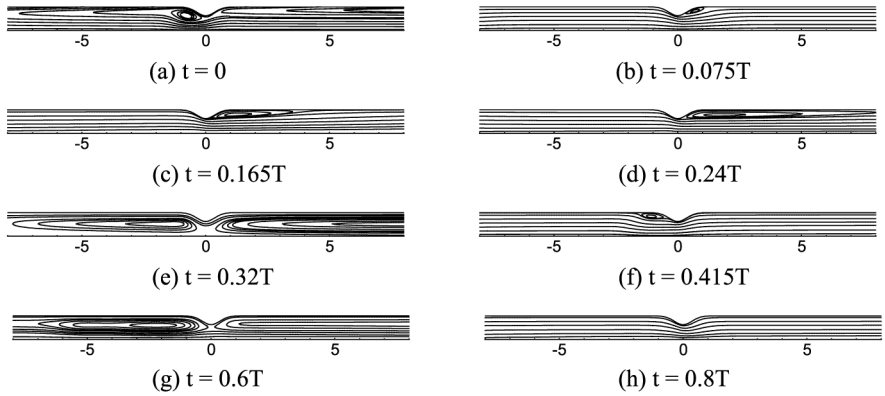

Figure 21.
The instantaneous streamlines in the tube with a stenosis at Re = 200 for the physiological flow

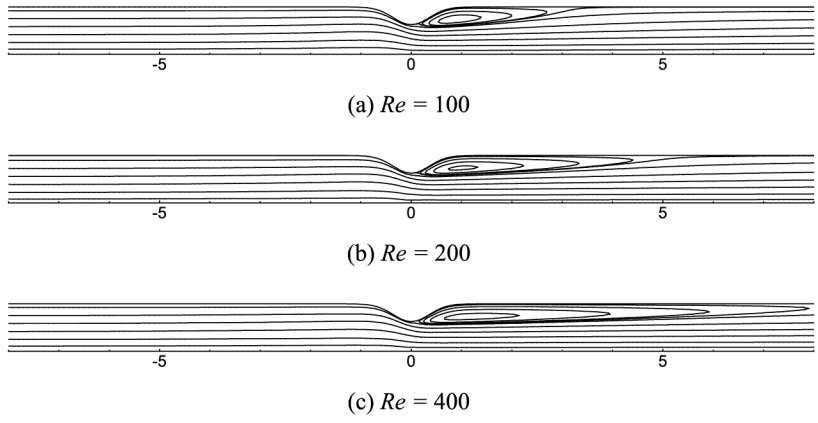

Figure 22.
Mean flow characteristics by averaging in time over one cycle at different Reynolds numbers for the physiological flow

Therefore, the high Reynolds number leads to the large instantaneous and mean peak wall vorticity.

So, the variation of the Reynolds number can significantly affect the flow behaviours for the physiological pulsatile flow. Generally, the strength and size of the vortex caused by stenosis grows with the increasing Reynolds number. The high Reynolds number can cause peak wall vorticity to increase evidently. The variation of Reynolds number has analogous influences on the time-averaged flow characteristics for the physiological pulsatile flow with those for steady flows.

6. Conclusions

The numerical solutions to three types of pulsatile flows through a bell-shaped arterial stenosis have been obtained in the present study. The detailed analysis on the characteristics of laminar flows over an arterial stenosis under the physiological flow conditions, including the comparison of the physiological pulsatile flow and two other pulsatile flows and the effects that some important flow parameters put on the physiological flow fields in stenosed arteries, is presented in this paper.

The comparison of the three pulsatile flows shows that the flow patterns of the physiological flow have distinct differences from those of the other two pulsatile flows while the flow patterns of the other two flows are similar to each other. At the instants where the net flow rate is zero, the recirculation zones always prefer to simultaneously occur at both proximal and distal to the stenosis for these pulsatile flows. For the physiological flow, therefore, the large recirculation zones that fill most of the flow field appear more frequently. It can be found that the flow field characteristics of the three pulsatile flows are very similar at the peak forward flow rate while at the peak backward flow rate, the magnitudes of negative peak values of the flow variables examined for the physiological flow are always much less than those for the other two pulsatile flows. Furthermore, the peak values and variation range of mean and instantaneous wall vorticity for the equivalent and simple pulsatile flow are

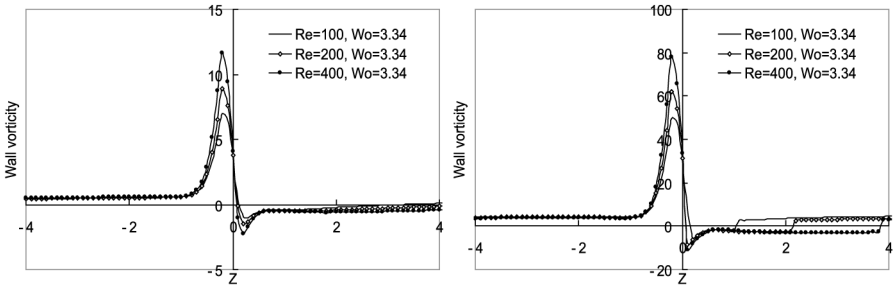

(a) Time-average wall vorticity (b) Maximum instantaneous wall vorticity

Figure 23.
The wall vorticity distribution in one cycle at different Reynolds numbers for the physiological flow

larger than those for the physiological flow. So the flow characteristics cannot be properly estimated if the equivalent or simple pulsatile inlet flow is used in the study of pulsatile arterial flow through stenosis instead of actual physiological one.

The structure of the flow fields for different constriction ratios has no significant differences under the current flow conditions except that more severe stenoses may lead to larger and stronger vortices in the flow field. The peak value and variation range of wall vorticity in one cycle depends monotonically on the constriction ratio c. The severe stenosis can cause wall vorticity to grow rapidly. Similarly, the pressure has greater variation ranges at most instants with the increasing constriction ratio. Generally, severe stenosis will make the flow variables vary more sharply. The Womersly number has significant effects on the unsteady flow field. With the Womersley number increasing, the structure of the flow field becomes more complex and there are more attached vortices to form. Furthermore, the values of the pressure vary in a greater range in one cycle and the pressure drop through the stenosis becomes slightly larger with the increasing Womersley number. However, the Womersley number has relatively small effects on the wall vorticity. The vortex development in the physiological flow field is strongly dependent on the variation of the Womersley number. At the corresponding instant during systole, the reattachment length reduces with the increasing Womersley number. During the deceleration phase of systole, the vortex may continue to grow in size and move downstream. The variation of the Reynolds number puts a great impact on the flow behaviors of the physiological pulsatile flow. Usually, the strength and size of the vortex caused by stenosis grow with the increasing Reynolds number. The high Reynolds number can cause peak wall vorticity to increase evidently. The variation of the Reynolds number has analogous influences on the time-averaged flow characteristics for the physiological pulsatile flow with those for steady flows.

References

Back, L.D., Radbill, J.R. and Crawford, D.W. (1977), "Analysis of pulsatile, viscous blood flow through diseased coronary arteries of man", *J. Biomech.*, Vol. 10, pp. 339-53.

Chorin, A.J. (1967), "A numerical method for solving incompressible viscous flow problems", *J. Comput. Phys.*, Vol. 2, pp. 12-26.

Daly, B.J. (1976), "A numerical study of pulsatile flow through stenosed canine femoral arteries", *J. Biomech.*, Vol. 9, pp. 465-75.

Deplano, V. and Siouffi, M. (1999), "Experimental and numerical study of pulsatile flows through stenosis: wall shear stress analysis", *J. Biomech.*, Vol. 32, pp. 1081-90.

Deshpande, M.D., Giddens, D.P. and Mabon, R.F. (1976), "Steady laminar flow through modeled vascular stenoses", *J. Biomech.*, Vol. 9, pp. 165-74.

Hirsch, C. (1990), *Numerical Computation of Internal and External Flows*, Wiley, New York, NY.

Huang, H., Modi, V.J. and Seymour, B.R. (1995), "Fluid mechanics of stenosed arteries", *Int. J. Eng. Sci.*, Vol. 33, pp. 815-28.

Lee, T.S. (1990), "Numerical studies of fluid flow through tubes with double contrictions", *Int. J. Numer. Methods Fluids*, Vol. 11, pp. 1113-26.

Lee, T.S. (1994), "Steady laminar fluid flow through variable constrictions in vascular tubes", *J. Fluids Eng.*, Vol. 116, pp. 66-71.

Lee, J.S. and Fung, Y.F. (1970), "Flow in locally constricted tubes at low Reynolds numbers", *ASME J. Appl. Mech.*, Vol. 37, pp. 9-16.

Lee, T.S., Liao, W. and Low, H.T. (2001), "Development of an artificial compressibility methodology with implicit LU-SGS method", *Int. J. Comp. Fluid Dynamics*, Vol. 15, pp. 197-208.

McDonald, D.A. (1955), "The relation of pulsatile pressure to flow in arteries", *J. Physiol.*, Vol. 127, pp. 533-52.

O'Brien, V. and Ehrlich, L.W. (1985), "Simple pulsatile flow in an artery with a constriction", *J. Biomech.*, Vol. 18, pp. 117-27.

Roe, P.L. (1981), "Approximate Riemann solvers, parameter, vectors, and difference schemes", *J. Comput. Phys.*, Vol. 43, pp. 357-72.

Siegel, J.M., Markou, C.P., Ku, D.N. and Hanson, S.R. (1994), "A scaling law for wall shear rate through an arterial stenosis", *J. Biomech. Eng. Trans. ASME*, Vol. 116, pp. 446-51.

Tu, C. and Deville, M. (1996), "Pulsatile flow of non-Newtonian fluids through arterial stenoses", *J. Biomech.*, Vol. 29, pp. 899-908.

Tu, C., Deville, M., Dheur, L. and Vanderschuren, L. (1992), "Finite element simulation of pulsatile flow through arterial stenosis", *J. Biomech.*, Vol. 25, pp. 1141-52.

Zendehbudi, G.R. and Moayeri, M.S. (1999), "Comparison of physiological and simple pulsatile flows through stenosed arteries", *J. Biomech.*, Vol. 32, pp. 959-65.